Polymer Journal (2018) 50:221–229
https://doi.org/10.1038/s41428-017-0007-5

ORIGINAL ARTICLE

Enhanced self-assembly of block copolymers by surface modification of a guiding template

Woon Ik Park[1,2] · Young Joong Choi[3] · Jong Min Yuk[4] · Hyeon Kook Seo[4] · Kwang Ho Kim[2,3]

Received: 21 August 2017 / Revised: 16 October 2017 / Accepted: 23 October 2017 / Published online: 19 December 2017
© The Society of Polymer Science, Japan 2018

Abstract

The formation of highly ordered patterns of block copolymers (BCPs) with high χ is important for next-generation lithography applications. We demonstrate here a surface-engineering methodology to enhance the self-assembly of poly (styrene-*b*-dimethylsiloxane) (PS-*b*-PDMS) BCPs with high χ by employing a hydroxyl-terminated polystyrene (PS-OH) brush. By precisely controlling the molecular weight (MW) and weight percent of PS-OH, well-ordered sub-20-nm BCP patterns were obtained over a large area in a short annealing time (<10 min) with the use of guiding templates. We systemically analyzed how the PS-OH brush affects the self-assembly kinetics of BCPs with various MWs and volume fractions. Moreover, the transmission electron microscopy (TEM) results strongly support that the PS-modulated surface plays an important role in the ordering of BCP patterns. We also achieved well-aligned 12 nm line and 18 nm dot patterns within 3 min by means of binary solvent vapor annealing at a moderate temperature under the optimum PS-OH brush conditions. These results provide a new platform for effective engineering and manipulation of the self-assembly of other BCPs for advanced BCP nanotechnologies.

Introduction

Over the last several decades, the directed self-assembly (DSA) of block copolymers (BCPs) has been intensively studied as a promising methodology for next-generation lithography due to its excellent pattern resolution, outstanding scalability, simple process, and good cost effectiveness [1–14]. BCPs, which consist of two or more mutually immiscible polymeric components can spontaneously self-assemble into periodic patterns, for example, dot, line, hole, and ring patterns, with small feature sizes of 5–50 nm through minimization of the Gibbs free energy [5, 8, 9, 12,14–19]. BCPs with a large Flory–Huggins interaction parameter (χ), in particular, have many advantages, including a low thermodynamic defect density, excellent pattern resolution, and morphological tunability, resulting from the large segregation strength (χN, N = degree of polymerization) of the high-χ BCP [5, 9, 17, 20, 21]. However, high-χ BCPs show slow self-assembly kinetics owing to the poor chain mobility, which decreases exponentially in proportion to the value of χ [21–23]. For this reason, high-χ BCPs typically require solvent vapor annealing to provide sufficient mobility to the BCP chains [24, 25]. In the literature, the efforts of many BCP research groups to develop novel and simple annealing methods to improve the self-assembly speed of high-χ BCPs are presented. These methods include thermally assisted solvent annealing and immersion annealing [19, 23, 26–29].

Woon Ik Park and Young Joong Choi authors are contributed equally to this work.

Electronic supplementary material The online version of this article (https://doi.org/10.1038/s41428-017-0007-5) contains supplementary material, which is available to authorized users.

✉ Kwang Ho Kim
thane0428@gmail.com
kwhokim@pusan.ac.kr

1 Electronic Convergence Materials Division, Korea Institute of Ceramic Engineering & Technology (KICET) 101 Soho-ro, Jinju 52851, Republic of Korea

2 Global Frontier R&D Center for Hybrid Interface Materials (GFHIM), Busandaehak-ro 63beon-gil, Geumjeong-gu, Busan 609-735, Republic of Korea

3 School of Materials Science and Engineering, Pusan National University (PNU), Busandaehak-ro 63beon-gil, Geumjeong-gu, Busan 609-735, Republic of Korea

4 Department of Materials Science and Engineering, Korea Advanced Institute of Science and Technology (KAIST) 291 Daehak-ro, Yuseong-gu, Daejeon 305-701, Republic of Korea

However, several critical issues remain unaddressed, such as the long-range ordering, defect density, and controllability, for a wider range of applications of high-χ BCPs to DSA. Prior to the annealing of BCP thin films, the substrate surface must be modified to obtain well-ordered BCP patterns and to control the geometry or orientation of the self-assembled BCP over the large area [6, 30]. Hence, many research groups have investigated the brush process to realize the formation of rapid and well-controlled patterns of highly ordered nanostructures. In general, the substrate is uniformly modified by a polymer brush treatment to promote the self-assembly of BCPs, such as homopolymers, random copolymers, mixed homopolymers, and block copolymers, showing a preference for one component of the BCP or neutral characteristics for di-BCPs. Harrison et al. [30] reported a PS brush process that involved anchoring the hydroxyl terminus of the brushes to the native oxide of the wafer, thereby modifying the affinity of the BCPs for the substrate by changing the wetting conditions of the substrate. Mansky et al. [31] found that the surface energy of the substrate can be tuned by adjusting the composition of a hydroxyl-terminated random copolymer to expedite the orientation of the BCP pattern. Kim et al. also demonstrated the controllability of the orientation of BCP microdomains using a self-assembled monolayer (SAM) or random copolymer brush, which can be grafted onto the substrate to form a neutrally modified surface [32]. However, these approaches are not suitable for high-χ BCPs, such as poly(2-vinylpyridine-*b*-dimethylsiloxane) (P2VP-*b*-PDMS), poly (styrene-*b*-dimethylsiloxane) (PS-*b*-PDMS), poly(styrene-*b*-ethylene oxide) (PS-*b*-PEO), poly(styrene-*b*-2-vinylpyridine) (PS-*b*-P2VP), poly(styrene-*b*-lactide) (PS-*b*-PLA) or poly(isoprene-*b*-lactide) (PI-*b*-PLA) [6, 11, 17, 33–39], owing to the large difference in the surface energy of each block. Related to this, Gu et al. recently suggested a new approach to control the alignment of BCPs with high χ using a surface modified with a hydroxyl-terminated BCP, depending on the composition of the anchored BCP brushes [40]. Despite these great efforts, there are remaining challenges to be addressed for actual applications of DSA in industry. In particular, systematic studies and a fundamental understanding of surface engineering to determine the self-assembly kinetics of high-χ BCPs based on the solvent annealing process are still lacking. Therefore, the systematic demonstration of a synergistic enhancement effect on the polymer chain mobility by both surface modification and solvent plasticization would be helpful to improve the self-assembly of high-χ BCPs.

Here we introduce a simple and novel surface modification method to enhance the self-assembly of BCPs with high χ using a hydroxyl-terminated polystyrene homopolymer (PS-OH) (PS brush) based on the solvent annealing system. In particular, we analyzed the effects of a PS brush on the self-assembly kinetics of PS-*b*-PDMS BCPs with a high χ (~0.26) depending on the molecular weight (MW) and weight percent. The key roles of the PS brush with regard to the defect density and self-assembly kinetics of BCPs were rationally demonstrated based on physical analyzes by thin film reflectometry, transmission electron microscopy (TEM), energy-dispersive X-ray spectroscopy (EDS), and scanning electron microscopy (SEM). In addition, we realized the rapid pattern formation of well-ordered sub-20-nm BCP patterns by employing a binary solvent mixture composed of toluene (a PS-preferential solvent) and heptane (a PDMS-preferential solvent) under the optimized PS brush conditions.

Materials and Methods

BCP self-assembly

To guide the self-assembly of the BCPs, Si substrates with line/space trenches with a depth of 40 nm and a width of 1 µm were fabricated using KrF photolithography. After the surface modification of the Si substrate by hydroxyl-terminated PS or PDMS homopolymers at 150 °C for 2 h in a vacuum oven, the substrates were washed with toluene to remove any unreacted polymer residue. All BCPs (SD28 and SD56) and homopolymers (PS-OH and PDMS-OH) in this study were purchased from Polymer Source Inc. (Canada). PS-OH polymers with MWs of 1 kg per mol, 38 kg per mol, and 130 kg per mol were used to promote the self-assembly of BCPs, showing good polydispersity indexes (PDI = Mw/Mn, Mn: number average molecular weight, Mw: weight average molecular weight) of 1.13, 1.09, and 1.07, respectively. The BCP solutions were spin-coated and annealed by warm solvent vapors at an annealing temperature of 55 °C. For the SEM images, the BCP samples were etched by CF_4 plasma (etching time = 25 s, gas flow rate = 30 sccm, working pressure = 15 mTorr, and plasma source power = 60 W) followed by O_2 plasma (etching time = 30 s, gas flow rate = 30 sccm, working pressure = 15 mTorr, and plasma source power = 60 W) to obtain the oxidized PDMS nanostructures (SiO_x), with an RIE process after the annealing process.

Transmission electron microscopy analysis

All transmission electron microscopy (TEM) images of the self-assembled PS-*b*-PDMS and PS-*b*-PFS microdomains were taken before the two-step plasma treatment, showing the PDMS or PFS microdomains in the PS matrix on the PS brush. The cross-sectional TEM samples were prepared by a mechanical polishing process, followed by ion milling with Ar ions. A high-resolution TEM analysis was conducted

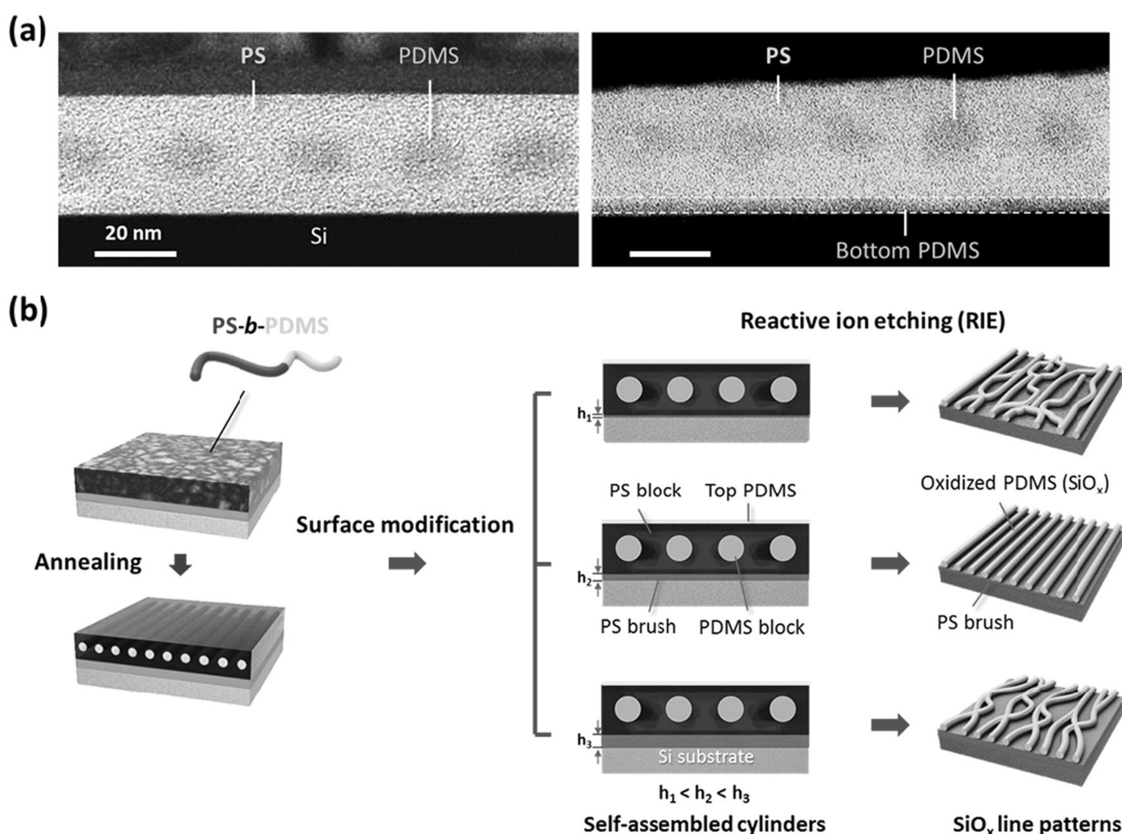

Fig. 1 Cross-sectional TEM morphologies of BCPs and conceptual illustrations of surface modification by the PS brush. **a** Comparison of self-assembled SD56 microdomains using different surface modifications with PS (left) and PDMS (right) brushes. **b** Conceptual description of the effect of the PS thickness on the ordering of self-assembled PS-*b*-PDMS BCPs after surface modification by the PS brush. The optimum thickness (h_2) of the PS wetting layer can enhance BCP self-assembly, resulting in a well-ordered pattern after a short annealing time (Color figure online)

using a JEOL JEM-ARM200F microscope operated at 200 kV.

Polymer film thickness measurement

The film thickness of the swollen BCP with/without PS brushes was measured by a reflectometry system with a wavelength range of 380–1050 nm (Filmetrics Inc., F20-UV, USA) by employing the reflectance method, which can measure the amount of light reflected from a polymer film. To obtain the swelling ratio (SR) of the thin polymer film, after measuring the initial and solvent-swollen thicknesses of the film, the initial thickness was divided by the swollen thickness.

Measurement of defect density

The self-assembled SiO_x patterns were observed by using field emission scanning electron microscopy (FE-SEM, Hitachi S-4800) operated with an acceleration voltage of 8 kV, emission current of 8 μA, and a working distance of 4 mm. We analyzed the SEM images of a cylinder-forming BCP pattern. We manually counted the number of defects (junctions and terminal points) using ImageJ software, according to the typical method as previously reported [26].

Results

Si-containing PS-*b*-PDMS BCPs are widely used for nanolithography and nanodevice applications owing to both the high-χ value and the highly etch-resistant PDMS block. PDMS preferentially segregates on top of the PS-*b*-PDMS BCP (air/polymer interface) to reduce the total surface energy after an annealing process due to the large difference in the surface energy between the PDMS ($\gamma = 19.9$ mN/m) and the PS ($\gamma = 40.7$ mN/m) [41]. To explain the role of the surface chemistry, Fig. 1a shows cross-sectional TEM morphologies of self-assembled BCPs with different polymer-surface interfaces when using a PS brush and a PDMS brush (PDMS-OH). A sphere-forming PS-*b*-PDMS with a MW of 56 kg per mol (SD56, $f_{PDMS} = 18.0\%$) was used for TEM analysis. When the PS brush was used, it (left image) can be homogeneously blended with the PS matrix,

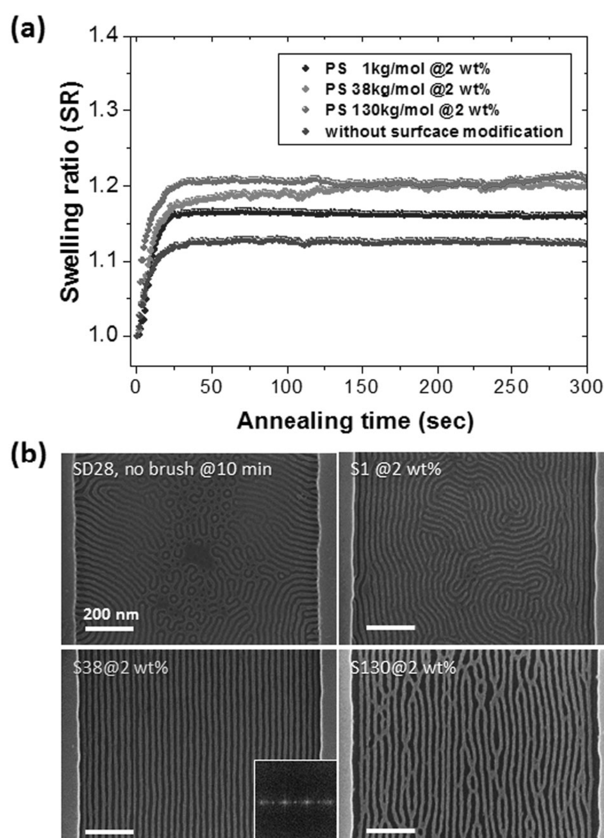

Fig. 2 Controlled self-assembly of PS-*b*-PDMS BCPs by engineering the molecular weight of the PS brush at 2.0 wt%. **a** Measurement of the swelling ratios (SRs) of SD28 BCPs depending on the MW of the PS brush. The annealing time was fixed at 10 min, while the MW was varied. **b** Self-assembled SD28 morphologies for different MWs of the PS brush (Color figure online)

whereas a PDMS surface layer (right image) was observed at the bottom (or on the surface of the substrate) when a PDMS brush (PDMS-OH) instead of the PS brush was used. The substrate coated with the PDMS brush often shows a non-uniform and irregular interface between the bottom PDMS layer and the substrate, as shown in Fig. 1a (right) and Supplementary Fig. S1 in Supporting Information. It is likely that PDMS, as the minority block of the di-BCP, can preferentially wet the substrate [30]. In addition, oxidized PDMS (ox-PDMS, SiO_x) directly formed on the bottom electrode coated with the PDMS brush, which shows resistive switching behavior and can be a disadvantage in electronic device applications [42]. Thus, the PS brush, as the majority block of the di-BCP, shows a physically uniform surface, which can be beneficial for BCP lithography and device applications. Figure 1b shows conceptual illustrations of the ordering of self-assembled PS-*b*-PDMS BCPs after surface modification by the PS brush. To expedite the self-assembly of PS-*b*-PDMS BCPs, we manipulated the thickness of the PS wetting layer by precisely controlling the MW and weight percent of the PS-OH homopolymer. In general, the thickness of the PS brush increases in proportion with the MW or weight percent, affecting the ordering of the self-assembled BCPs and their annealing time. The optimum thickness (h_2) of the PS wetting layer can enhance the BCP self-assembly, resulting in a highly ordered nanostructure after a short annealing time. On the other hand, an insufficient and excessively thick PS layer (h_3 and h_1) disturbs the self-assembly of BCPs, resulting in poorly ordered BCP patterns.

First, to explore the influence of the thickness of the PS brush on BCP self-assembly, we measured the swelling ratio (SR = swollen thickness/initial thickness) of cylinder-forming PS-*b*-PDMS with a MW of 28 kg per mol (SD28, $f_{PDMS} = 32.1\%$) and various MWs of the PS brush annealed with pure toluene. All of the PS-OH polymers were dissolved in toluene at 2 wt% and spin-coated onto a guiding template, which were then annealed in a vacuum oven at 150 °C for 2 h and washed with toluene. The SR of the SD28 BCP thin film increased in proportion to the MW of the PS-OH homopolymer, as shown in Fig. 2a. This is likely attributed to the incorporation of toluene molecules into the SD28 and PS layer film, depending on the MW of the PS brush or the thickness of PS residue. The SR curve of the PS brush with a MW of 130 kg per mol (S130) shows a slightly higher value (~1.21) than that (~1.20) of the PS brush with a MW of 38 kg per mol (S38). The SR curve of SD28 modified with a PS brush with a small MW of 1 kg per mol (S1) shows a smaller SR value (~1.16) than those of the S38 and S130 brushes, resulting from the non-uniform brush coverage, as shown in Supplementary Fig. S2b. The SR curve of the BCP thin film without any surface modification (bare Si) displays a low SR value (~1.12). These results clearly show that the PS layer anchored to the surface of the substrate is swollen by toluene (solubility parameter of toluene, $\delta_{Tol} = 18.3\ MPa^{1/2}$), which is a good solvent for PS polymers.

Figure 2b shows the self-assembled SD28 morphologies for PS brushes with different MWs at a fixed annealing time of 10 min. SD28 on a substrate treated with a S1 polymer brush shows a disordered structure with dots, in-plane lines, and holes, similar to the result without brush treatment (Supplementary Fig. S5). Supplementary Fig. S3 shows the time evolution of the self-assembled SD28 formed on the S1 brush, showing poorly ordered line structures. However, when the S1 brush had a higher weight percentage (10 wt %), the ordering of SD28 was improved, as shown in Supplementary Fig. S3c. These results imply that the thickness of the PS residue affects the PS-*b*-PDMS BCP ordering, and therefore, an unreasonably short PS chain length can cause the disordering of PS-*b*-PDMS BCPs, even though the grafting density is sufficiently high. SD28 modified with a S130 brush forms an entangled line pattern, showing a poorly ordered structure even after a long

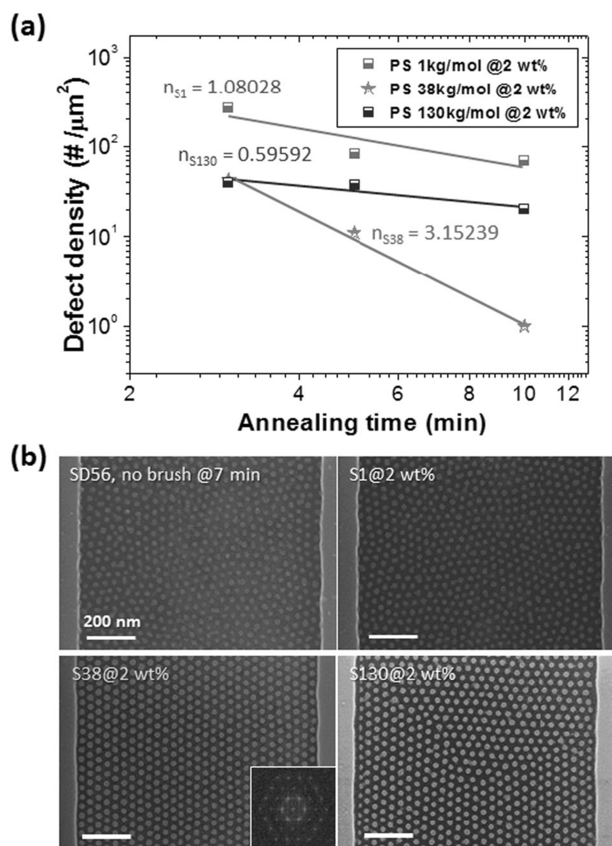

Fig. 3 Comparison of the defect density for various MWs of the PS brush, and the similar MW effect for sphere-forming SD56 BCPs. **a** Graph of the defect density vs. annealing time for SD28 BCPs depending on the MW of the PS brush at 2.0 wt%. **b** Self-assembled SD56 morphologies at different MWs of the PS brush with a fixed annealing time of 7 min. The inset in the SEM images displays the fast Fourier transforms (FFTs) of each self-assembled morphology (Color figure online)

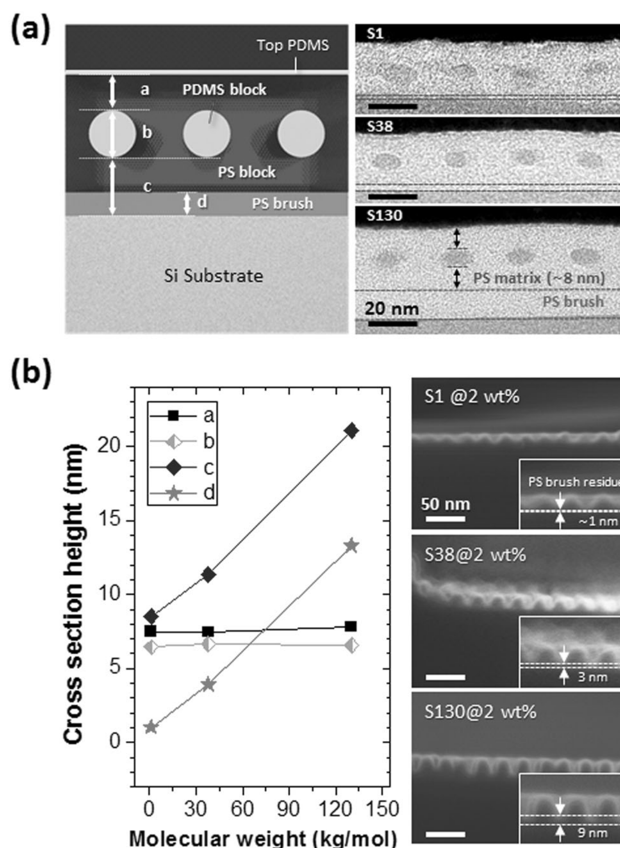

Fig. 4 Analyzes of the self-assembled cylinder-forming SD28 BCP morphologies after engineering the film thickness of the PS brush. All TEM images show the cross-sectional morphologies of the SD28 BCPs. **a** (Left) Cross-sectional schematic diagram of a cylinder-forming PS-*b*-PDMS BCP thin film formed on the PS-modified substrate, which indicates the distances between the top PDMS and the PDMS microdomain. (Right) Cross-sectional TEM morphologies of the self-assembled SD28 BCPs on a guiding template surface-treated with PS brushes with different MWs (S1, S38, and S130). **b** (Left) Analysis graph of the thickness for the TEM data of **a**. (Right) Cross-sectional SEM images show self-assembled SD28 line patterns with different MWs of the PS brush after etching by an RIE system (Color figure online)

annealing time (60 min), as shown in Fig. 2b, Supplementary Fig. S3. This result suggests that BCPs treated by PS-OH with an excessively large MW (S130) can disrupt BCP self-assembly, despite the sufficient swelling of the BCP. On the other hand, the S38 brush successfully formed a well-ordered line pattern. The ordering of the self-assembled BCP patterns after surface modification clearly shows a relation between the defect density (D) and annealing time (t), which is expressed as $D \sim t^{-n}$. As shown in Fig. 3a, the reduction in the defect density for the S38 brush is much steeper than those of the S1 and S130 brushes. The time-decay exponent (n) for the S1, S38, and S130 brushes was estimated to be 1.08, 3.15, and 0.60, respectively, indicating that surface modification with the S38 brush can significantly reduce the defect density or increase the ordering of SD28 BCPs. Similarly, the sphere-forming SD56 BCP shows a similar trend for the defect density, forming a well-organized 20-nm dot pattern when using the S38 brush after annealing for 7 min (Fig. 3b). These results suggest that the use of PS-OH (S38) with similar chain lengths and a majority of PS blocks of PS-*b*-PDMS BCPs (e.g., SD28 and SD56) may be more favorable for the ordering of BCP microdomains than using PS-OH with extremely long PS chains (e.g., S130).

The image on the left in Fig. 4a shows a cross-sectional schematic diagram of a cylinder-forming PS-*b*-PDMS BCP thin film formed on a PS-modified substrate, indicating the distance between the top PDMS and the PDMS microdomain (a), the height of the PDMS microdomain (b), the distance between the PDMS microdomain and the substrate (c), and the thickness of the PS brush residue (d). The images on the right in Fig. 3a present the cross-sectional TEM morphologies of self-assembled SD28 BCPs on a guiding template surface-treated with PS brushes with

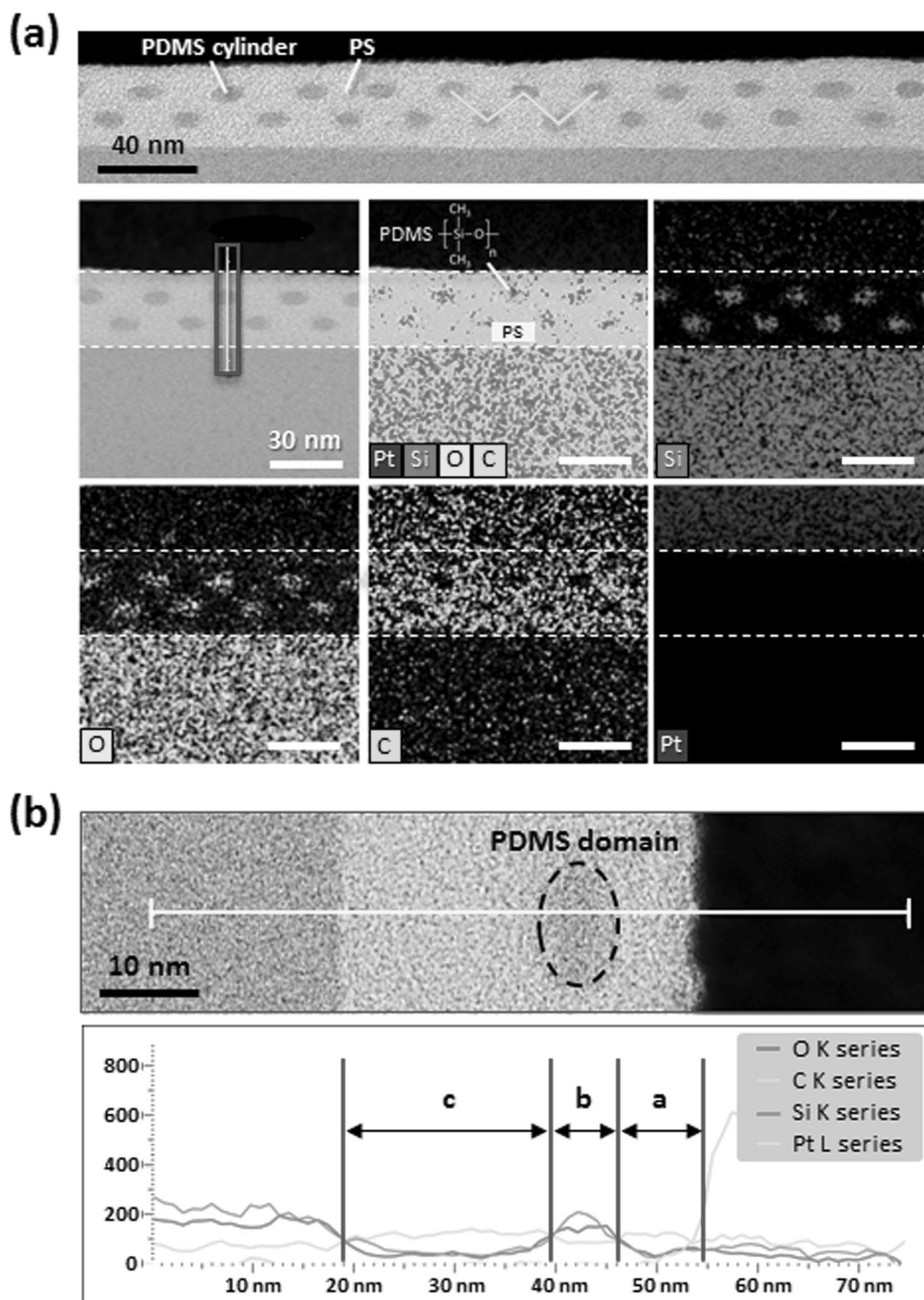

Fig. 5 Elemental mapping of the self-assembled SD28 bilayer cylinders on the S38 brush. **a** Cross-sectional TEM and EDS elemental mapping images for highly ordered bilayer cylinders of SD28 at 1.2 wt% on the S38 brush. **b** Qualitative analysis of each element of the self-assembled SD28 sample, showing line profiles of the O, C, Si, and Pt atoms. Pt was deposited only to fabricate the TEM samples (Color figure online)

different MWs (S1, S38, and S130), showing the different film thickness before the selective removal of the PS block of the BCP. The total film thickness (=a+b+c) or the thickness of the PS brush residue ($d \cong$ c−a) increases in proportion to the PS chain length, which depends on the MW of the PS homopolymer, as shown in Fig. 4a (right) and Fig. 4b. The cross-sectional SEM images in Fig. 4b shows self-assembled SD28 line patterns after etching with CF_4 plasma followed by O_2 plasma treatment using an ion reactive etching (RIE) system; these images also show a similar dependency on the MW of the PS brush (corresponding to the results before dry etching). The S1 brush shows a very small PS brush height (d = ~1 nm) due to its short chain length and poor surface coverage, which was expected. When the S38 brush is used, the TEM and SEM morphologies show an optimized height of ~3 nm, with sharper and more well-defined PDMS microdomains than those of the S1 brush, stemming from the formation of perfectly ordered PDMS cylinders. SD28 treated with the S130 brush has a thicker PS layer (~9 nm) owing to its longer chain length than those of S1 and S38. To obtain a well-ordered BCP pattern with the S130 brush, a thinner

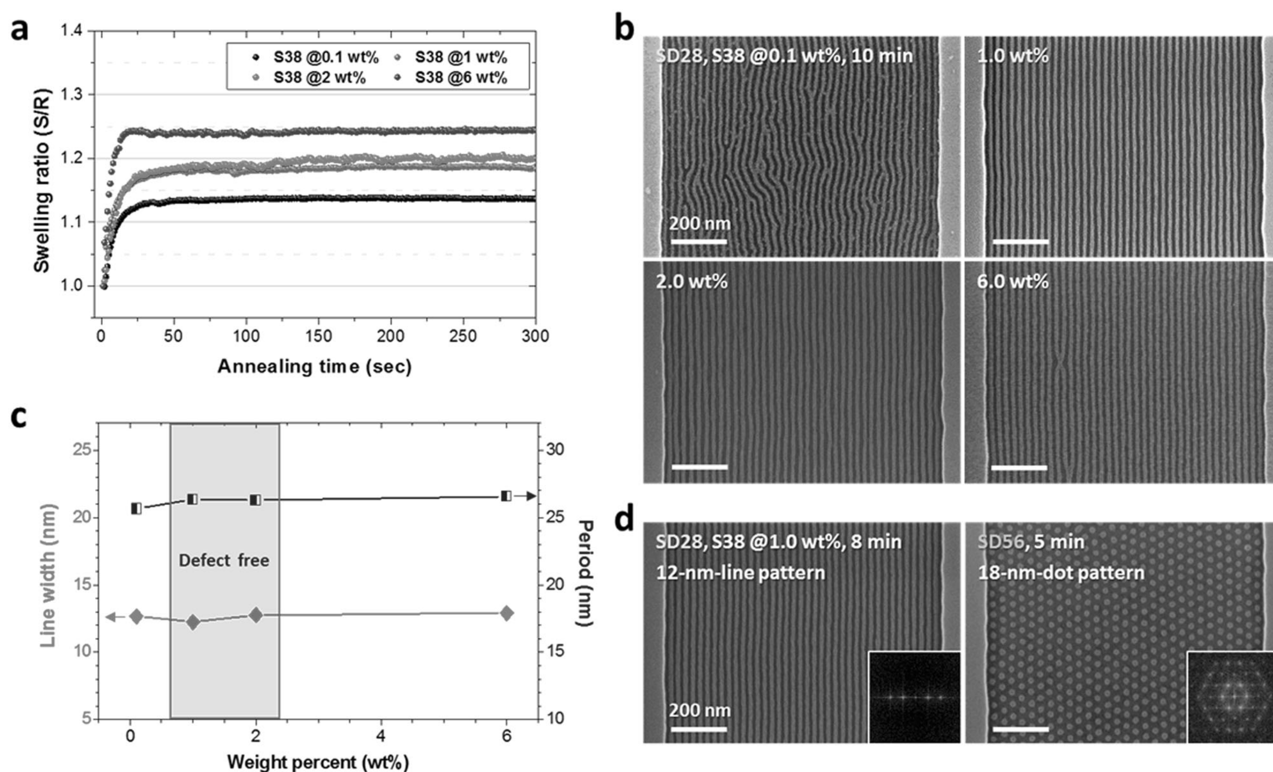

Fig. 6 Controlled self-assembly of PS-*b*-PDMS BCPs by modifying the weight percent of the S38 polymer. **a** Comparison of the swelling ratios of the SD28 thin film depending on the weight percent of the S38 brush with pure toluene vapor. The graph shows the proportional increase in the SR value with an increase in the weight percent. **b** SEM images of self-assembled SD28 patterns with various weight percentages when annealed in toluene vapor at a fixed annealing time of 10 min. **c** Graph of the line width and pattern period of **b**. **d** Self-assembled SD28 and SD56 patterns when using 1 wt% S38 brush. The inset images are FFTs of each SEM image (Color figure online)

film thickness of the BCP may be required. Figure 5a shows cross-sectional TEM and EDS elemental mapping images of highly ordered SD28 bilayer cylinders on the S38 brush obtained with a thick BCP film (1.2 wt%) layer when annealed under the optimum annealing conditions. The high density of Si and O in the PDMS block and the excellent ordering of the SD28 cylinders provides extremely high elemental contrast. Although many research groups had difficulty measuring the oxygen and carbon content in the BCPs by EDS analysis, we successfully obtained the EDS elemental mapping data for the double density of cylinder structures induced by the S38 brush, distinctly showing O and C in the images from the qualitative analysis, as demonstrated in the bottom of Fig. 5a (left and middle) and Fig. 5b. Therefore, we emphasize that clear Si, O, and C mapping results are valuable in the fields of microscopy and polymers.

We also investigated the effects of the thickness or weight percent of the S38 polymer on the self-assembly of SD28 BCP. Figure 6a shows the SR curves of SD28 with various weight percentages (0.1–6.0 wt%) of the S38 brush, showing a proportional increase in the SR value with an increase in the weight percent. As described above, it is also likely, in this case as well, that the residual PS layer beneath the BCP film can be swollen by PS-preferential toluene vapor. At an extremely low weight percent of 0.1 wt%, the SR has a very low value (~1.13) due to its poor coverage of the surface, similar to the result with the S1 brush (Supplementary Figs. S2, S4a). SD28 on S38 at 0.1 wt% formed a poorly ordered line pattern with many defects at an annealing time of 10 min (Fig. 6b, top left image). After a long annealing time (30 min), a disordered pattern with film damage or dewetting caused by toluene vapor was observed, as shown in Supplementary Fig. S4b (upper image). On the other hand, using the S38 brush at 6.0 wt% results in high swelling of the film (~1.24) and a relatively well-ordered line pattern (bottom right image in Fig. 6b and bottom image in Supplementary Fig. S4b). The SD28 BCP treated with 1.0 wt% and 2.0 wt% S38 showed relatively high SRs of ~1.19 and ~1.2, respectively (Fig. 6a), which resulted in well-ordered patterns (top right and bottom left images in Fig. 6b). These results are likely due to the uniformly covered surface after the brush process (Supplementary Fig. S4). Supplementary Fig. 6c shows a graph of the line width and pattern period when using S38 at various weight percentages, resulting in no noticeable differences in the dimensions of the SD28 patterns. We also achieved the pattern formation of highly ordered 12-nm line (SD28) and 18-nm dot (SD56) patterns at annealing times of 8 min and

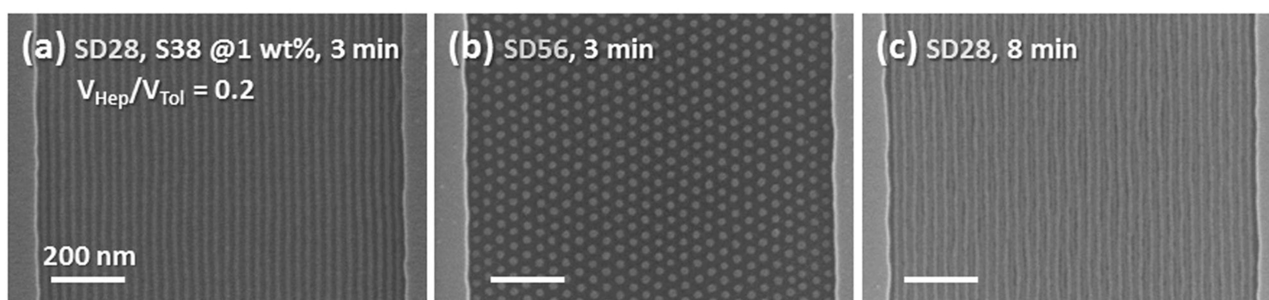

Fig. 7 Ultra-fast pattern formation of SD28 and SD56 BCPs with a binary solvent mixture composed of heptane and toluene. Well-ordered nanostructures of **a** SD28 at 0.6 wt%, **b** SD56 at 0.6 wt%, and **c** SD28 at 1.2 wt%. The SD28 and SD56 BCPs can be effectively self-assembled into periodic line and dot patterns within 3 min when $V_{Hep}/V_{Tol} = 0.2$. The bilayer line pattern of the SD28 BCP was obtained when $V_{Hep}/V_{Tol} = 0.2$ with an annealing time of 8 min (Color figure online)

5 min, respectively, under the optimum PS brush conditions (1 wt% S38) (Fig. 6d). Figure S6 in Supporting Information displays the time evolution of the self-assembled SD56 for the S1 and S130 brushes, showing poorly ordered patterns compared to the S38 brush. These results strongly support that the MW of the PS brush affects the ordering of the self-assembled BCPs.

Finally, we realized the ultra-rapid pattern formation of BCPs by employing a binary solvent annealing method under the optimum PS brush conditions. A binary solvent mixture composed of a PS-preferential solvent (toluene) and a PDMS-preferential solvent (heptane) for PDMS-*b*-PS BCPs can induce extremely rapid self-assembly kinetics, as we previously reported. As shown in Fig. 7, the generation of well-ordered periodic line and dot (0.6 wt% SD28 and SD56) patterns was accomplished within a very short annealing time of 3 min with a mixture of heptane and toluene at a heptane-to-toluene mixing ratio of 0.2 ($V_{Hep}/V_{Tol} = 0.2$). Moreover, a highly ordered bilayer line pattern (1.2 wt% SD28) was successfully obtained in 8 min. It should also be noted that the ordering and annealing time of the self-assembled BCP can be further reduced by adopting narrower guiding templates based on this combination of surface modification and binary solvent annealing.

Conclusions

In summary, we introduced a facile and practical surface-engineering method to increase the self-assembly kinetics of PS-*b*-PDMS BCPs with high χ by employing a hydroxyl-terminated PS homopolymer. We systematically showed how well-ordered sub-20-nm BCP patterns can be obtained with the guiding templates in a short annealing time (<10 min) by precisely controlling the molecular weight and weight percent (or film thickness) of the PS brush. The TEM, EDS elemental mapping, and SEM results clearly indicate that the PS-modified surface plays a key role in the rapid and convenient formation of well-ordered BCPs, indicating the optimum conditions of the PS brush. In addition, we successfully achieved ultra-fast pattern formation (<3 min) of highly ordered sub-20-nm BCPs using a binary solvent annealing method under the optimum PS brush conditions. This approach is expected to be extended to various high-χ BCPs, providing new opportunities to effectively modulate BCP self-assembly for next-generation sub-10-nm lithography applications.

Acknowledgments This research was supported by the Global Frontier Program through the Global Frontier Hybrid Interface Materials (GFHIM) of the National Research Foundation of Korea (NRF) funded by the Ministry of Science, ICT and Future Planning. (No. 2013M3A6B1078874).

Author contributions W.I.P., Y.J.C, and K.H.K. conceived the experiments. W.I.P. and Y.J.C. performed the self-assembly experiments. W.I.P. and Y.J.C. analyzed SEM data. H.K.S. and J.M.Y. contributed to the analysis of the TEM data. W.I.P. and Y.J.C. wrote the majority of the paper. All authors contributed to discussions and writing of the paper.

Compliance with ethical standards

Conflict of interest The authors declare that they have no competing financial interests.

References

1. Segalman RA, Yokoyama H, Kramer EJ. Graphoepitaxy of spherical domain block copolymer films. Adv. Mater. 2001;13:1152–5.
2. Kim SO, Solak HH, Stoykovich MP, Ferrier NJ, De Pablo JJ, Nealey PF. Epitaxial self-assembly of block copolymers on lithographically defined nanopatterned substrates. Nature. 2003;424:411–4.
3. Cheng JY, Mayes AM, Ross CA. Nanostructure engineering by templated self-assembly of block copolymers. Nat. Mater. 2004;3:823–8.
4. Stoykovich MP, Muller M, Kim SO, Solak HH, Edwards EW, de Pablo JJ et al. Directed assembly of block copolymer blends into nonregular device-oriented structures. Science. 2005;308:1442–6.

5. Black CT, Ruiz R, Breyta G, Cheng JY, Colburn ME, Guarini KW et al. Polymer self assembly in semiconductor microelectronics. IBM J. Rev. Dev. 2007;51:605–33.
6. Jung YS, Ross CA. Orientation-controlled self-assembled nanolithography using a polystyrene-polydimethylsiloxane block copolymer. Nano Lett. 2007;7:2046–50.
7. Yang JK, Jung YS, Chang JB, Mickiewicz RA, Alexander-Katz A, Ross CA et al. Complex self-assembled patterns using sparse commensurate templates with locally varying motifs. Nat. Nanotechnol. 2010;5:256–60.
8. Darling SB. Directing the self-assembly of block copolymers. Prog. Poly. Sci. 2007;32:1152–204.
9. Bates CM, Seshimo T, Maher MJ, Durand WJ, Cushen JD, Dean LM et al. Polarity-switching top coats enable orientation of sub-10-nm block copolymer domains. Science. 2012;338:775–9.
10. Bita I, Yang JKW, Jung YS, Ross CA, Thomas EL, Berggren KK. Graphoepitaxy of self-assembled block copolymers on two-dimensional periodic patterned templates. Science. 2008;321:939–43.
11. Park S, Lee DH, Xu J, Kim B, Hong SW, Jeong U et al. Macroscopic 10-terabit-per-square-inch arrays from block copolymers with lateral order. Science. 2009;323:1030–3.
12. Ruiz R, Kang HM, Detcheverry FA, Dobisz E, Kercher DS, Albrecht TR et al. Density multiplication and improved lithography by directed block copolymer assembly. Science. 2008;321:936–9.
13. Tang C, Lennon EM, Fredrickson GH, Kramer EJ, Hawker CJ. Evolution of block copolymer lithography to highly ordered square arrays. Science. 2008;322:429–32.
14. Tavakkoli KGA, Gotrik KW, Hannon AF, Alexander-Katz A, Ross CA, Berggren KK. Templating three-dimensional self-assembled structures in bilayer block copolymer films. Science. 2012;336:1294–8.
15. Chai J, Wang D, Fan XN, Buriak JM. Assembly of aligned linear metallic patterns on silicon. Nat. Nanotechnol. 2007;2:500–6.
16. Ross CA, Berggren KK, Cheng JY, Jung YS, Chang JB. Three-dimensional nanofabrication by block copolymer self-assembly. Adv. Mater. 2014;26;4386–96.
17. Jeong JW, Park WI, Kim MJ, Ross CA, Jung YS. Highly tunable self-assembled nanostructures from a poly(2-vinylpyridine-b-dimethylsiloxane) block copolymer. Nano Lett. 2011;11:4095–101.
18. Park WI, Kim Y, Jeong JW, Kim K, Yoo JK, Hur YH et al. Host-guest self-assembly in block copolymer blends. Sci. Rep. 2013;3:3190.
19. Park WI, Kim JM, Jeong JW, Jung YS. Deep-nanoscale pattern engineering by immersion-induced self-assembly. ACS Nano. 2014;8:10009–18.
20. Leibler L. Theory of microphase separation in block copolymers. Macromol. 1980;13:1602–17.
21. Lodge TP, Dalvi MC. Mechanisms of chain diffusion in lamellar block copolymers. Phys. Rev. Lett. 1995;75:657–60.
22. Bates FS, Fredrickson GH. Block copolymer thermodynamics: theory and experiment. Annu. Rev. Phys. Chem. 1990;41:525–57.
23. Park WI, Kim K, Jang HI, Jeong JW, Kim JM, Choi J et al. Directed self-assembly with sub-100 degrees celsius processing temperature, sub-10 nanometer resolution, and sub-1 minute assembly time. Small. 2012;8:3762–8.
24. Kim SH, Misner MJ, Xu T, Kimura M, Russell TP. Highly oriented and ordered arrays from block copolymers via solvent evaporation. Adv. Mater. 2004;16:226–31.
25. Jung YS, Ross CA. Solvent-vapor-induced tunability of self-assembled block copolymer patterns. Adv. Mater. 2009;21:2540–5.
26. Zhang X, Harris KD, Wu NL, Murphy JN, Buriak JM. Fast assembly of ordered block copolymer nanostructures through microwave annealing. ACS Nano. 2010;4:7021–9.
27. Gotrik KW, Ross CA. Solvothermal annealing of block copolymer thin films. Nano Lett. 2013;13:5117–22.
28. Borah D, Shaw MT, Holmes JD, Morris MA. Sub-10 nm feature size PS-b-PDMS block copolymer structures fabricated by a microwave-assisted solvothermal process. ACS Appl. Mater. Interface. 2013;5:2004–12.
29. Park WI, Choi YJ, Yun JM, Hong SW, Jung YS, Kim KH. Enhancing the directed self-assembly kinetics of block copolymers using binary solvent mixtures. ACS Appl. Mater. Interface 2015;7:25843–50.
30. Harrison C, Chaikin PM, Huse DA, Register RA, Adamson DH, Daniel A et al. Reducing substrate pinning of block copolymer microdomains with a buffer layer of polymer brushes. Macromol. 2000;33:857–65.
31. Mansky P, Liu Y, Huang E, Russell TP, Hawker CJ. Controlling polymer-surface interactions with random copolymer brushes. Science. 1997;275:1458–60.
32. Jeong S-J, Xia G, Kim BH, Shin DO, Kwon SH, Kang S-W et al. Universal block copolymer lithography for metals, semiconductors, ceramics, and polymers. Adv. Matter. 2008;20:898–1904.
33. Jung YS, Chang JB, Verploegen E, Berggren KK, Ross CA. A path to ultranarrow patterns using self-assembled lithography. Nano Lett. 2010;10:1000–5.
34. Hammond MR, Cochran E, Fredrickson GH, Kramer EJ. Temperature dependence of order, disorder, and defects in laterally confined diblock copolymer cylinder monolayers. Macromol. 2005;38:6575–85.
35. Jang SG, Khan A, Hawker CJ, Kramer EJ. Morphology evolution of PS-b-P2VP diblock copolymers via supramolecular assembly of hydroxylated gold nanoparticles. Macromol. 2012;45:1553–61.
36. Zalusky AS, Olayo-Valles R, Wolf JH, Hillmyer MA. Ordered nanoporous polymers from polystyrene-polylactide block copolymers. J. Am. Chem. Soc. 2002;124:12761–73.
37. Keen I, Cheng HH, Yu AG, Jack KS, Younkin TR, Leeson MJ et al. Behavior of lamellar forming block copolymers under nanoconfinement: implications for topography directed self-assembly of sub-10 nm structures. Macromol. 2014;47:276–83.
38. Keen I, Yu AG, Cheng HH, Jack KS, Nicholson TM, Whittaker AK et al. Control of the orientation of symmetric poly(styrene)-block-poly(D,L-lactide) block copolymers using statistical copolymers of dissimilar composition. Langmuir. 2012;28:15876–88.
39. Cavicchi AK, Russell PT. Solvent annealed thin films of asymmetric polyisoprene-polylactide diblock copolymers. Macromol. 2007;40:1181–6.
40. Gu W, Hong SW, Russell TP. Orienting block copolymer microdomains with block copolymer brushes. ACS Nano. 2012;6:10250–7.
41. Chan CM. Polymer surface modification and characterization. New York, Hanser Publishers, 1st edn (1994).
42. Park WI, You BK, Mun BH, Seo HK, Lee JY, Hosaka S et al. Self-assembled incorporation of modulated block copolymer nanostructures in phase-change memory for switching power reduction. ACS Nano. 2013;7:2651–8.